Growth of Ionic Polymers on ZIFs to Construct Core-shell Hybrid Materials via Coordination Interactions for Catalytic CO_2 Conversion

Jinquan Wang,[a]* Xiukai Li,[a] Siew Ping Teong,[a] Shook Pui Chan,[a] Zibiao Li[a], Xinglong Zhang[b]* and Yugen Zhang[a]*

[a]Institute of Sustainability for Chemicals, Energy and Environment (ISCE2), Agency for Science, Technology and Research (A*STAR), 1 Pesek Road Jurong Island, Singapore 627833.

[b]Department of Chemistry, The Chinese University of Hong Kong, Shatin, New Territories, Hong Kong, China

***corresponding e-mail:** wang_jinquan@a-star.edu.sg, xinglong.zhang@cuhk.edu.hk, zhang_yugen@a-star.edu.sg

4. COMPUTATIONAL SECTION

4.1 Computational Methods

The model catalyst was conformationally sampled to locate the most stable complex. The conformational sampling was carried out using Grimme's *CREST* program[1,2], which used metadynamics (MTD) with genetic z-matrix crossing (GC) performed at the GFN2-xTB[3–5] extended semiempirical tight-binding level of theory with *opt= vtight* option. Ten of the lowest energy GFN2-xTB optimized structures from the CREST search were further optimized using density functional theory (DFT), implemented in *Gaussian 16* rev. B.01 software[6], in the gas phase using the B3LYP hybrid functional[7–10] with Grimme's D3 dispersion correction with Becke-Johnson damping[11] (hereafter denoted B3LYP-D3BJ) and the def2-SVPD[12,13] Karlsruhe-family basis set for Br atom and def2-SVP[12,14] basis set for all other atoms (this mixed basis set is denoted BS1). The "D" in def2-SVPD basis set denotes diffuse functions which are important for the correct description of anionic electron distributions [15-17]. Dispersion correction (D3BJ) has been added to correctly capture non-covalent interactions [18-21]. Minima and transition structures on the potential energy surface (PES) were confirmed as such by harmonic frequency analysis, showing respectively zero and one imaginary frequency.

Gibbs energies were evaluated at the reaction temperature of 110 °C, using Grimme's scheme of quasi-RRHO treatment of vibrational entropies [22], using the GoodVibes code [23]. Vibrational entropies of frequencies below 100 cm^{-1} were obtained according to a free rotor description, using a smooth damping function to interpolate between the two limiting descriptions [22].

The free energies reported in *Gaussian* from gas-phase optimization were further corrected using standard concentration of 1 mol/L [24], which were used in solvation calculations, instead of the gas-phase 1atm used by default in the *Gaussian* program.

To improve on the accuracy of the corrected Gibbs energy profile, single point (SP) calculations on the gas phase B3LYP-D3BJ/BS1 optimized geometries were performed at B3LYP-D3BJ with def2-TZVPD[12,13] basis set for Br atom and def2-TZVP[12,14] basis set for all other atoms (denoted BS2) in the implicit SMD continuum solvation model[25] for ethanol solvent that was used experimentally, to account for the effect of solvent on the potential energy surface. The final corrected Gibbs energy SMD(ethanol)-B3LYP-D3BJ/BS2//B3LYP-D3BJ/BS1 is used for discussion throughout. All Gibbs energy values in the text and figures are quoted in kcal mol^{-1}.

Non-covalent interactions (NCIs) were analyzed using NCIPLOT[26] calculations. The *.wfn* files for NCIPLOT were generated at BS1 level of theory. NCI indices calculated with NCIPLOT were visualized at a gradient isosurface value of *s = 0.5* au. These are colored according to the sign of the second eigenvalue (λ_2) of the Laplacian of the

density ($\nabla^2\rho$) over the range of –0.1 (blue = attractive) to +0.1 (red = repulsive). Molecular orbitals are visualized using an isosurface value of 0.05 au throughout. All molecular structures and molecular orbitals were visualized using *PyMOL* software [27].

4.2 Model reaction

Scheme S1 shows the model reaction that we have used for the computational studies of reaction mechanism for ZIF catalyzed conversion of CO_2 and epoxide to cyclic carbonate. Model catalyst **INT1** was used to represent the full catalyst **ZP2**.

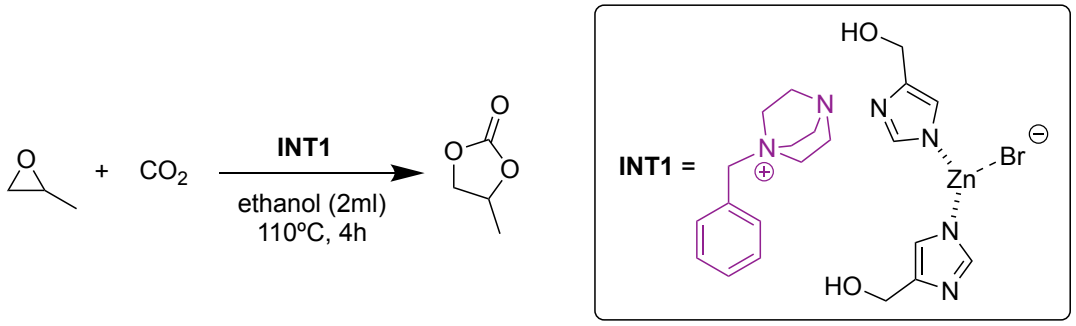

Scheme S1. Model reaction used in the computational modelling studies.

The DFT optimized transition state (TS) structures for the model reaction are shown in Fig. S13.

TS1	**TS2**
$\Delta G^{\ddagger}$ = 20.8	$\Delta G^{\ddagger}$ = 17.2
Im. Freq = 294.6278 *i*	Im. Freq = 81.2937 *i*
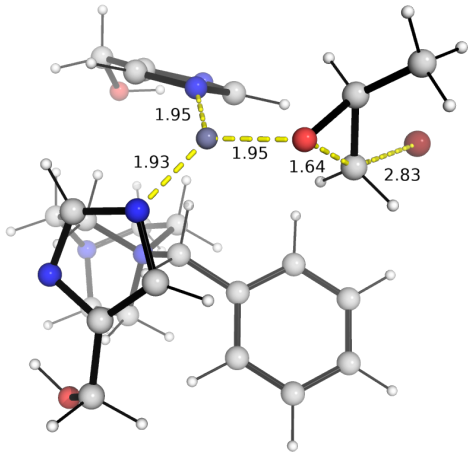	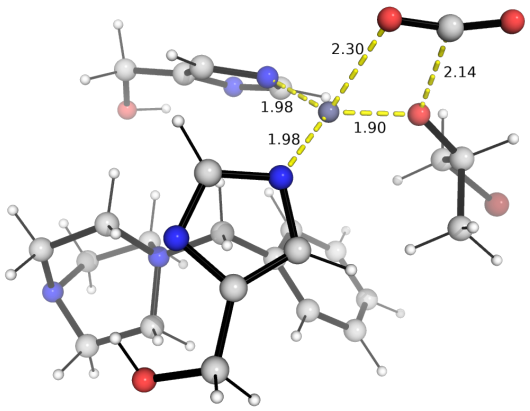
TS3	
$\Delta G^{\ddagger}$ = 22.6	
Im. Freq = 427.8558 *i*	

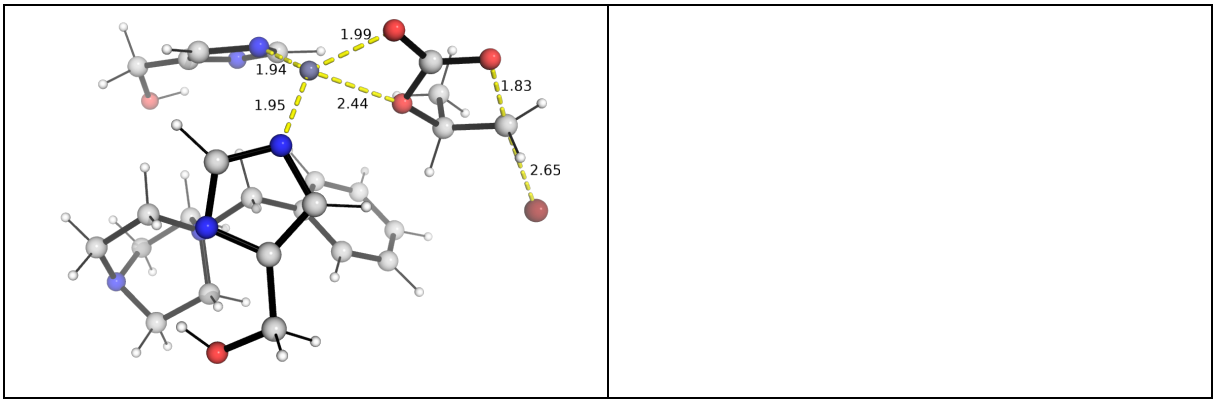

Figure S13. DFT optimized structures for the model reaction shown in Scheme S1. Key distances are given in Å.

4.3 Role of hydroxyl (OH) groups

To understand the role of the hydroxyl groups on the catalyst, we replaced the OH groups by H atom to get the model reaction shown in Scheme S2 top; we also model the catalyst ZP1 by INT1b shown in Scheme S2 bottom.

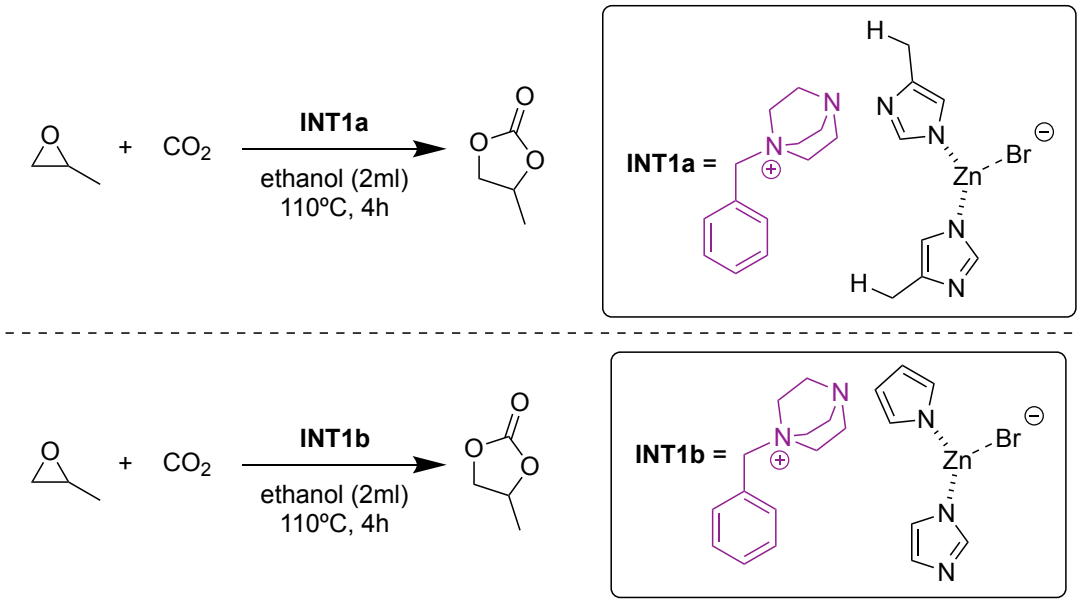

Scheme S2. Reaction where the hydroxyl groups in the catalyst is replaced by H atoms.

We focused on the ring closure step, which is the rate-determining step. We calculated the energies of the turnover frequency (TOF)-determining intermediate (TDI), which is **INT1a** and **INT1b**, and the TOF-determining transition state (TDTS), which is the ring closure step (**TS3a** and **TS3b**, DFT optimized structure in Figure S5).

	TS3	**TS3a**	**TS3b**
$\Delta G^{\ddagger}$	22.6 kcal/mol	23.9 kcal/mol	23.6 kcal/mol
Im.Freq	427.8558 *i*	424.4198 *i*	424.8663 *i*

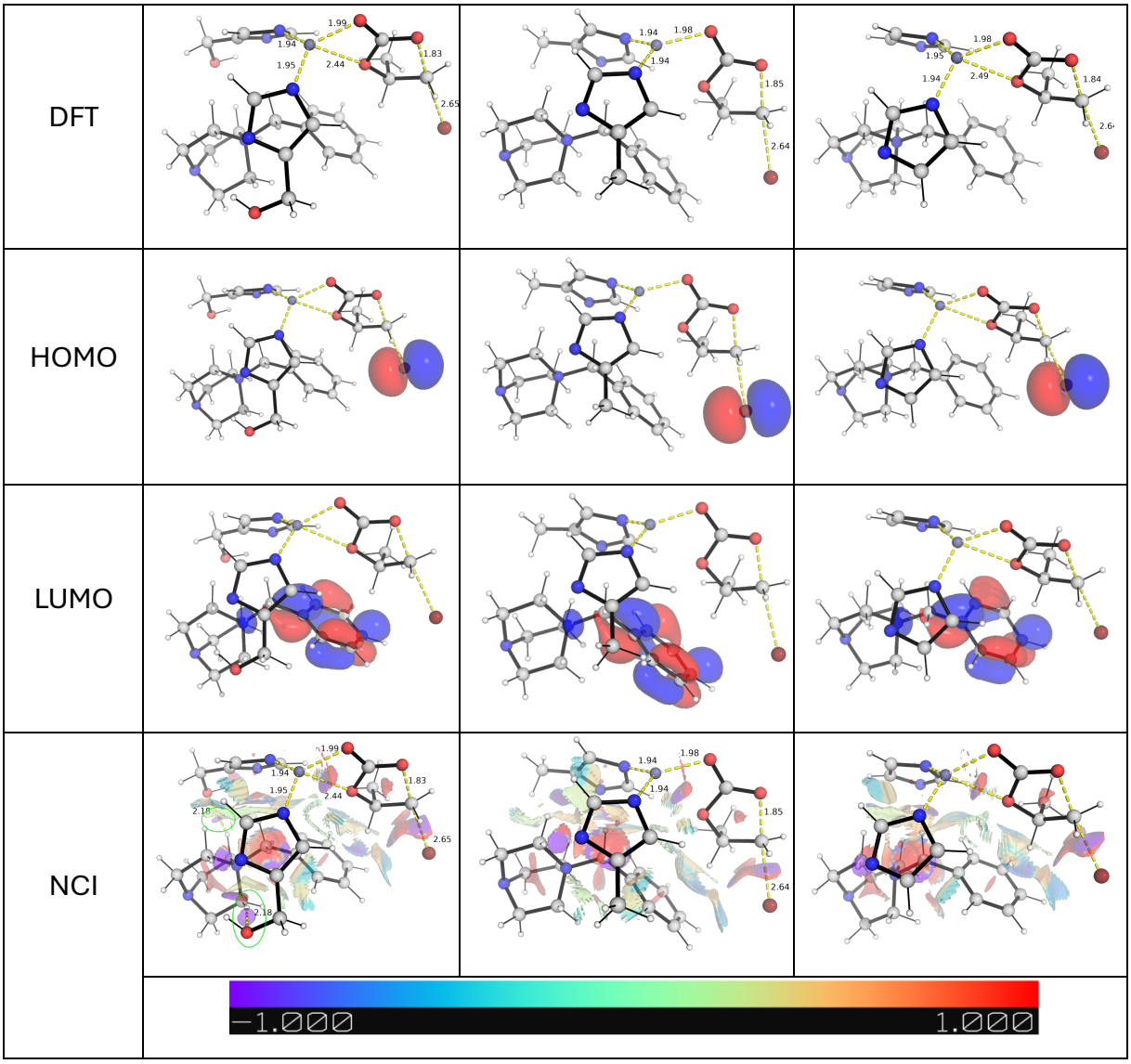

Figure S14. DFT optimized structures, frontier molecular orbitals (FMOs) and non-covalent interaction (NCI) plots for the ring closure step for **INT1** and **INT1'** catalysts. Key distances are given in Å.

4.4 Model reaction using polymer P1

To understand the role of the ZIF in the performance, we model the reaction using polymer **P1** shown in Scheme S3.

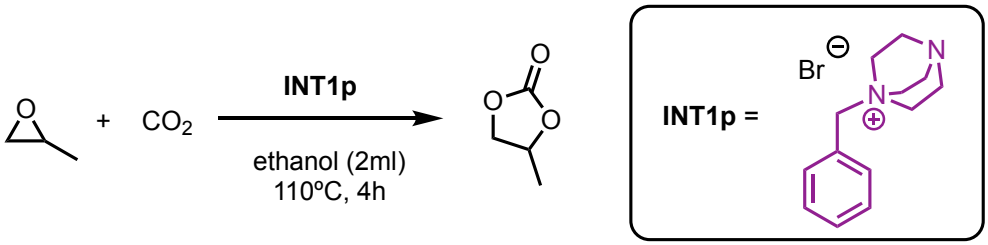

Scheme S2. Model reaction using polymer **P1**.

Since this polymer lacks Zn ions, the steps may have different barriers compared to the ZIF systems studied previously. As such, we performed computational studies on the full catalytic cycle. The Gibbs energy profile is shown in Figure S7.

We can see that the epoxide ring opening by bromide anion has a high barrier of 27.9 kcal/mol (**TS1p**, Fig. S7). This forms a ring-opened intermediate **INT3p**, that is highly exergonic. **INT3p** then adds to CO_2 without an appreciable barrier, as the direct optimization of **INT3p** in the presence of CO_2 (placed more than 5Å away) yields **INT5p** directly. This is then followed by ring closing **TS3p** (26.0 kcal/mol) to yield the final cyclic carbonate product.

We see that the ring opening of epoxide by bromide anion is the overall rate-determining step and this gives the energetic span of the catalytic reaction as 27.9 kcal/mol. This step is not favored, as in the absence of any Lewis acid activation, the epoxide is not very nucleophilic towards bromide attack.

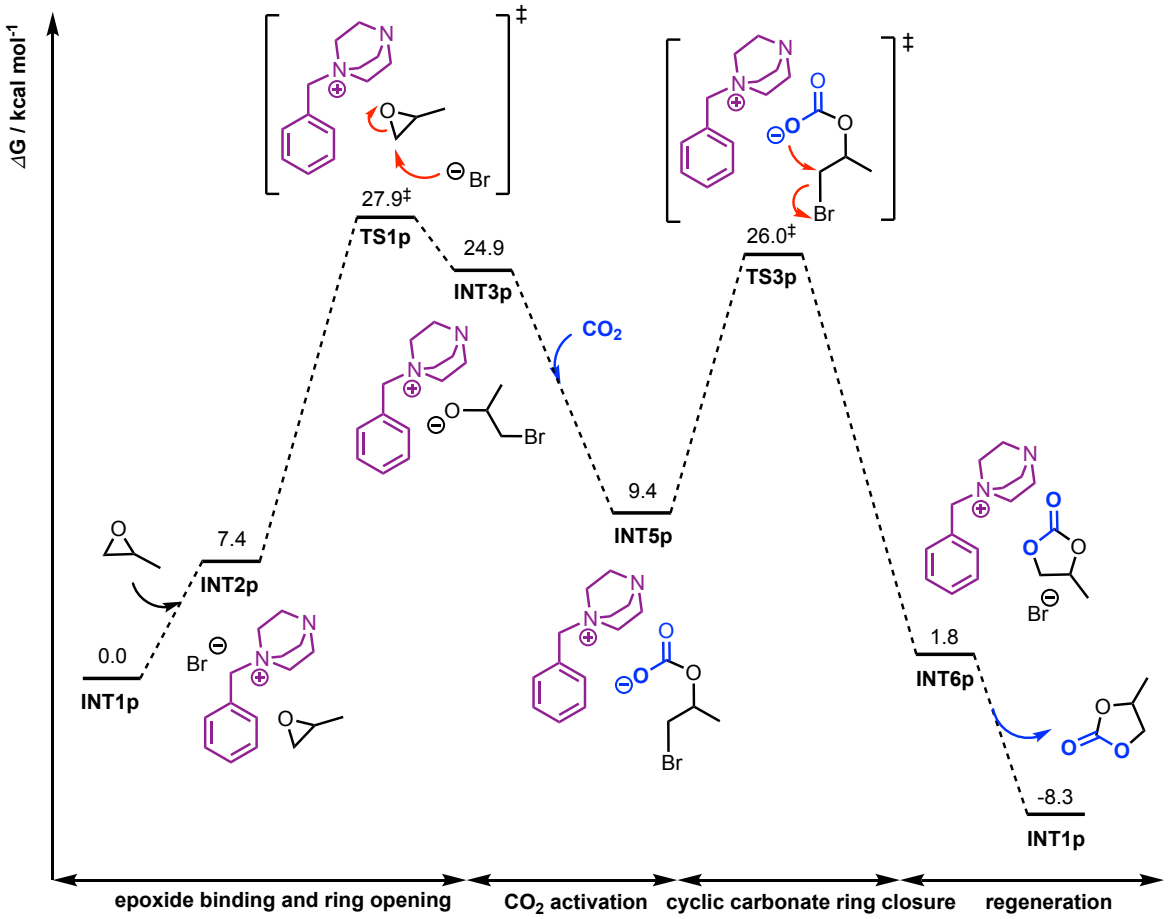

Figure S15 The Gibbs free energy profile for the formation of cyclic carbonate catalyzed by polymer **P1** modeled using **INT1p**.

4.5 Optimized structures and absolute energies, zero-point energies

Geometries of all optimized structures (in *.xyz* format with their associated energy in Hartrees) are included in a separate folder named *DFT_optimized_structures* with an associated readme.txt file. All these data have been deposited and uploaded to https://zenodo.org/records/13296902 (DOI: 10.5281/zenodo.13296902).

Absolute values (in Hartrees) for SCF energy, zero-point vibrational energy (ZPE), enthalpy and quasi-harmonic Gibbs free energy (at 110 °C/383.15 K) for optimized structures are given below. Single point corrections in SMD ethanol using B3LYP-D3/BS2 level of theory are also included.

Structure	E/au	ZPE/au	H/au	T.S/au	qh-G/au	SP B3LYP-D3/BS2
CO2	-188.44468	0.011776	-188.42806	0.028446	-188.456508	-188.6672
epoxide	-192.97454	0.085035	-192.88161	0.039452	-192.921056	-193.2052
cyclic_carbonate	-381.4548	0.102874	-381.34117	0.048034	-381.388858	-381.9099
INT1	-5648.9864	0.499023	-5648.4384	0.141014	-5648.567049	-5651.024722
INT1-c2	-5648.9864	0.499023	-5648.4384	0.141001	-5648.567044	-5651.024712
INT1-c3	-5648.9864	0.499023	-5648.4384	0.140994	-5648.567042	-5651.024701
INT1-c4	-5648.9864	0.499023	-5648.4384	0.140992	-5648.56704	-5651.024717
INT1-c5	-5648.9826	0.498632	-5648.4347	0.140902	-5648.563855	-5651.023719
INT1-c6	-5648.9806	0.498318	-5648.4329	0.142591	-5648.562902	-5651.02216
INT1-c7	-5648.9809	0.498326	-5648.4331	0.141982	-5648.562708	-5651.022758
INT1-c8	-5648.9788	0.498466	-5648.4321	0.13789	-5648.558984	-5651.017204
INT1-c9	-5648.9734	0.499792	-5648.4256	0.135607	-5648.551167	-5651.011303
INT2	-5841.9992	0.585977	-5841.3553	0.1622	-5841.502012	-5844.248011
TS1	-5841.9281	0.584605	-5841.2861	0.158384	-5841.430962	-5844.221108
INT3	-5841.975	0.586429	-5841.3314	0.15817	-5841.475614	-5844.250108

INT4	-6030.4381	0.599567	-6029.7758	0.172974	-6029.932092	-6032.91795
TS2	-6030.4379	0.599453	-6029.7769	0.168669	-6029.93018	-6032.916427
INT5	-6030.4495	0.602007	-6029.7864	0.16644	-6029.938194	-6032.939161
TS3	-6030.4118	0.601296	-6029.75	0.165722	-6029.901082	-6032.910897
INT6	-6030.4214	0.602935	-6029.7573	0.168921	-6029.91012	-6032.932912
INT1a	-5498.6545	0.486357	-5498.1213	0.134946	-5498.245244	-5500.519544
INT1a-c2	-5498.6528	0.486384	-5498.1195	0.136396	-5498.244232	-5500.5164
INT1a-c3	-5498.6528	0.486383	-5498.1195	0.136402	-5498.244235	-5500.516391
INT1a-c4	-5498.6528	0.486384	-5498.1195	0.136401	-5498.244236	-5500.516376
INT1a-c5	-5498.6522	0.486293	-5498.119	0.136005	-5498.243452	-5500.515339
TS3a	-5880.0800	0.588819	-5879.4328	0.160781	-5879.579779	-5882.403174
INT1b	-5420.0592	0.431524	-5419.586	0.124041	-5419.699923	-5421.840313
TS3b	-5801.4844	0.534071	-5800.8971	0.150077	-5801.034224	-5803.724306
INT1p	-3189.8039	0.307525	-3189.4721	0.081614	-3189.549687	-3190.826582
INT2p	-3382.8083	0.394796	-3382.3799	0.105065	-3382.476804	-3384.043692
INT2p-c2	-3382.8083	0.394796	-3382.3799	0.104852	-3382.476678	-3384.043567
INT2p-c3	-3382.8084	0.394917	-3382.38	0.104332	-3382.476653	-3384.043375
INT2p-c4	-3382.807	0.394534	-3382.3788	0.106309	-3382.476424	-3384.041532
INT2p-c5	-3382.8083	0.394716	-3382.3799	0.105411	-3382.477104	-3384.041818
INT2p-c6	-3382.8084	0.394625	-3382.3801	0.105148	-3382.477172	-3384.041706

INT2p-c7	-3382.8082	0.394654	-3382.3799	0.104802	-3382.47682	-3384.041496
INT2p-c8	-3382.8080	0.394812	-3382.3795	0.105986	-3382.476854	-3384.041233
INT2p-c9	-3382.8083	0.394899	-3382.3798	0.105	-3382.47671	-3384.041425
INT2p-c10	-3382.8083	0.394898	-3382.3798	0.104998	-3382.47671	-3384.041417
TS1p	-3382.7586	0.392916	-3382.3327	0.102244	-3382.42831	-3384.009755
INT3p	-3382.7763	0.393428	-3382.3501	0.101061	-3382.444765	-3384.015836
INT5p	-3571.2623	0.410299	-3570.8152	0.111193	-3570.918526	-3572.731854
TS3p	-3571.2378	0.410216	-3570.7918	0.107532	-3570.892659	-3572.706738
INT6p	-3571.2700	0.412051	-3570.8213	0.113213	-3570.925249	-3572.744981

4.6 References for computational section:

Full reference Gaussian 16:

Gaussian 16, Revision B.01, Frisch, M. J.; Trucks, G. W.; Schlegel, H. B.; Scuseria, G. E.; Robb, M. A.; Cheeseman, J. R.; Scalmani, G.; Barone, V.; Mennucci, B.; Petersson, G. A.; Nakatsuji, H.; Caricato, M.; Li, X.; Hratchian, H. P.; Izmaylov, A. F.; Bloino, J.; Zheng, G.; Sonnenberg, J. L.; Hada, M.; Ehara, M.; Toyota, K.; Fukuda, R.; Hasegawa, J.; Ishida, M.; Nakajima, T.; Honda, Y.; Kitao, O.; Nakai, H.; Vreven, T.; Montgomery Jr., J. A.; Peralta, J. E.; Ogliaro, F.; Bearpark, M.; Heyd, J. J.; Brothers, E.; Kudin, K. N.; Staroverov, V. N.; Kobayashi, R.; Normand, J.; Raghavachari, K.; Rendell, A.; Burant, J. C.; Iyengar, S. S.; Tomasi, J.; Cossi, M.; Rega, N.; Millam, J. M.; Klene, M.; Knox, J. E.; Cross, J. B.; Bakken, V.; Adamo, C.; Jaramillo, J.; Gomperts, R.; Stratmann, R. E.; Yazyev, O.; Austin, A. J.; Cammi, R.; Pomelli, C.; Ochterski, J. W.; Martin, R. L.; Morokuma, K.; Zakrzewski, V. G.; Voth, G. A.; Salvador, P.; Dannenberg, J. J.; Dapprich, S.; Daniels, A. D.; Farkas, Ö.; Foresman, J. B.; Ortiz, J. V; Cioslowski, J.; Fox, D. J. Gaussian, Inc., Wallingford CT, 2016.

[1] Grimme, S. Exploration of Chemical Compound, Conformer, and Reaction Space with Meta-Dynamics Simulations Based on Tight-Binding Quantum Chemical Calculations. *J. Chem. Theory Comput.* **2019**, *15* (5), 2847–2862.

[2] Pracht, P.; Bohle, F.; Grimme, S. Automated Exploration of the Low-Energy Chemical Space with Fast Quantum Chemical Methods. *Phys. Chem. Chem. Phys.* **2020**, *22* (14), 7169–7192.

[3] Bannwarth, C.; Ehlert, S.; Grimme, S. GFN2-XTB - An Accurate and Broadly Parametrized Self-Consistent Tight-Binding Quantum Chemical Method with Multipole Electrostatics and Density-Dependent Dispersion Contributions. *J. Chem. Theory Comput.* **2019**, *15* (3), 1652–1671.

[4] Grimme, S.; Bannwarth, C.; Shushkov, P. A Robust and Accurate Tight-Binding Quantum Chemical Method for Structures, Vibrational Frequencies, and Noncovalent Interactions of Large Molecular Systems Parametrized for All Spd-Block Elements (Z = 1-86). *J. Chem. Theory Comput.* **2017**, *13* (5), 1989–2009.

[5] Bannwarth, C.; Caldeweyher, E.; Ehlert, S.; Hansen, A.; Pracht, P.; Seibert, J.; Spicher, S.; Grimme, S. Extended Tight-Binding Quantum Chemistry Methods. *Wiley Interdiscip. Rev. Comput. Mol. Sci.* **2021**, *11* (2), e1493.

[6] Frisch, M. J. .; Trucks, G. W. .; Schlegel, H. B. .; Scuseria, G. E. .; Robb, M. A. .; Cheeseman, J. R. .; Scalmani, G. .; Barone, V. .; Petersson, G. A. .; Nakatsuji, H. .; et al. Gaussian 16, Revision B.01. 2016.

[7] Becke, A. D. Density-Functional Thermochemistry. III. The Role of Exact Exchange. *J. Chem. Phys.* **1993**, *98* (7), 5648–5652.

[8] Lee, C.; Yang, W.; Parr, R. G. Development of the Colle-Salvetti Correlation-Energy Formula into a Functional of the Electron Density. *Phys. Rev. B* **1988**, *37* (2), 785–789.

[9] Vosko, S. H.; Wilk, L.; Nusair, M. Accurate Spin-Dependent Electron Liquid Correlation Energies for Local Spin Density Calculations: A Critical Analysis. *Can. J. Phys.* **1980**, *58* (8), 1200–1211.

[10] Stephens, P. J.; Devlin, F. J.; Chabalowski, C. F.; Frisch, M. J. Ab Initio Calculation of Vibrational Absorption and Circular Dichroism Spectra Using Density Functional Force Fields. *J. Phys. Chem.* **1994**, *98* (45), 11623–11627.

[11] Grimme, S.; Antony, J.; Ehrlich, S.; Krieg, H. A Consistent and Accurate Ab Initio Parametrization of Density Functional Dispersion Correction (DFT-D) for the 94 Elements H-Pu. *J. Chem. Phys.* **2010**, *132* (15), 154104.

[12] Weigend, F.; Ahlrichs, R. Balanced Basis Sets of Split Valence, Triple Zeta Valence and Quadruple Zeta Valence Quality for H to Rn: Design and Assessment of Accuracy. *Phys. Chem. Chem. Phys.* **2005**, *7* (18), 3297–3305.

[13] Hellweg, A.; Rappoport, D. Development of New Auxiliary Basis Functions of the Karlsruhe Segmented Contracted Basis Sets Including Diffuse Basis Functions (Def2-SVPD, Def2-TZVPPD, and Def2-QVPPD) for RI-MP2 and RI-CC Calculations. *Phys. Chem. Chem. Phys.* **2014**, *17* (2), 1010–1017.

[14] Weigend, F. Accurate Coulomb-Fitting Basis Sets for H to Rn. *Phys. Chem. Chem. Phys.* **2006**, *8* (9), 1057–1065.

[15] Davidson, E. R.; Feller, D. Basis Set Selection for Molecular Calculations. *Chem. Rev.* **1986**, *86* (4), 681–696.

[16] Lynch, B. J.; Zhao, Y.; Truhlar, D. G. Effectiveness of Diffuse Basis Functions for Calculating Relative Energies by Density Functional Theory. *J. Phys. Chem. A* **2003**, *107* (9), 1384–1388.

[17] Papajak, E.; Zheng, J.; Xu, X.; Leverentz, H. R.; Truhlar, D. G. Perspectives on Basis Sets Beautiful: Seasonal Plantings of Diffuse Basis Functions. *J. Chem. Theory Comput.* **2011**, *7* (10), 3027–3034.

[18] Grimme, S. Density Functional Theory with London Dispersion Corrections. *Wiley Interdiscip. Rev. Comput. Mol. Sci.* **2011**, *1* (2), 211–228.

[19] Burns, L. A.; Vázquez-Mayagoitia, Á.; Sumpter, B. G.; Sherrill, C. D. Density-Functional Approaches to Noncovalent Interactions: A Comparison of Dispersion Corrections (DFT-D), Exchange-Hole Dipole Moment (XDM) Theory, and Specialized Functionals. *J. Chem. Phys.* **2011**, *134* (8).

[20] Dilabio, G. A.; Koleini, M. Dispersion-Correcting Potentials Can Significantly Improve the Bond Dissociation Enthalpies and Noncovalent Binding Energies Predicted by Density-Functional Theory. *J. Chem. Phys.* **2014**, *140* (18).

[21] Cohen, A. J.; Mori-Sánchez, P.; Yang, W. Challenges for Density Functional Theory. *Chem. Rev.* **2012**, *112* (1), 289–320.

[22] Grimme, S. Supramolecular Binding Thermodynamics by Dispersion-Corrected Density Functional Theory. *Chem.: Eur. J.* **2012**, *18* (32), 9955–9964.

[23] Luchini, G.; Alegre-Requena, J. V.; Funes-Ardoiz, I.; Paton, R. S. GoodVibes: Automated Thermochemistry for Heterogeneous Computational Chemistry Data. *F1000Research* **2020**, *9*, 291.

[24] Bryantsev, V. S.; Diallo, M. S.; Goddard Iii, W. A.; Goddard, W. A. Calculation of Solvation Free Energies of Charged Solutes Using Mixed Cluster/Continuum Models. *J. Phys. Chem. B* **2008**, *112* (32), 9709–9719.

[25] Marenich, A. V.; Cramer, C. J.; Truhlar, D. G. Universal Solvation Model Based on Solute Electron Density and on a Continuum Model of the Solvent Defined by the Bulk Dielectric Constant and Atomic Surface Tensions. *J. Phys. Chem. B* **2009**, *113* (18), 6378–6396.

[26] Contreras-García, J.; Johnson, E. R.; Keinan, S.; Chaudret, R.; Piquemal, J. P.; Beratan, D. N.; Yang, W. NCIPLOT: A Program for Plotting Noncovalent Interaction Regions. *J. Chem. Theory Comput.* **2011**, *7* (3), 625–632.

[27] Schrödinger, L. *The PyMOL Molecular Graphics Development Component, Version 1.8*; 2015.